Statistical and block conjugated polymers for bulk heterojunction solar cells: molecular orientation, charge transfer dynamics and device performance

Bianca Pedroso S. Santos[a], Roger S. Correa[b], Amanda G. Veiga[b], Emmanuel V. Péan[e], Bruno G. A. L. Borges[b], Francineide L. Araújo[d], Arthur C. Ribeiro[c], José G. M. Furtado[c], Matthew L. Davies[e,f], Ana F.Nogueira[c], Maria L. M. Rocco[b*], Maria F. V. Marques[a*]

[a] *Instituto de Macromoléculas Professora Eloisa Mano (IMA), Universidade Federal do Rio de Janeiro, Cidade Universitária, 21941-598, Rio de Janeiro, Brasil.*

[b] *Instituto de Química, Universidade Federal do Rio de Janeiro, CidadeUniversitária, 21941-909, Rio de Janeiro, Brasil.*

[c] *Centro de Pesquisas de Energia Elétrica (Cepel), CidadeUniversitária, 21941-911, Rio de Janeiro, Brasil*

[d]*Laboratório de Nanotecnologia e Energia Solar (LNES), Instituto de Química, Universidade de Campinas (UNICAMP), 13083-970, Campinas-São Paulo, Brasil.*

[e] *Specific IKC, Materials Research Centre, College of Engineering, Swansea University, UK*

[f] *School of Chemistry and Physics, University of KwaZulu-Natal, Durban, RSA.*

*Corresponding authors. *E-mail address:* fmarques@ima.com.br (Maria de Fátima Vieira Marques) and luiza@iq.ufrj.br (Maria Luiza M. Rocco)

Keywords: Block terpolymer, Statistical terpolymer, Photovoltaics, X-ray absorption spectroscopy, Core-Hole Clock method.

ABSTRACT

Two terpolymers based on fluorene, benzothiadiazole and carbazole monomer units were investigated as electron donor materials in organic solar cells. Variation of the microstructure, either statistical or in block, was shown to significantly affect the optoelectronic properties of the polymers. Both terpolymers presented a high open-circuit voltage in photovoltaic devices (ca. 0.8-0.95 V). Polymer solar cell assembled with the active layer composed of the statistical polymer in combination with PCBM exhibited good photovoltaic performance, with power

conversion efficiency (PCE) of 1.5% using chlorobenzene as solvent and annealing treatment of the active layer. In its turn, the block terpolymer showed the best result when the same solvent and the additive 1,8-diiodooctane (DIO) was used in the mixture. After introducing the additive in the preparation of the active layer, changing the solvent to dichlorobenzene and varying the ratio of donor to acceptor, *i.e.*, block polymer:$PC_{60}BM$, the device showed PCE of 1.2% and 2.2%, with ratio 1:2 and 1:1 w/w, respectively. In order to better understand the different devices performance spectroscopic techniques were employed in an attempt to gain information on the electronic structure, morphology and dynamics processes of charge transfer of the polymeric films.

1. Introduction

Bulk heterojunction (BHJ) is the most commonly used active layer architecture in organic photovoltaic (OPV). Fundamentally, the active layer is the layer in which the incident light is absorbed and photon energy is converted into electrical energy. Two components are mixed in the active layer forming an interpenetrating polymer network: an electron donor (typically a conjugated polymer, a p-type semiconductor) and an electron acceptor species (usually a fullerene derivative, acting as n-type semiconductor). Optimizing the morphology and inherent properties of this blended polymer layer is critical to optimize device performance, and to this end a great deal of research has been carried out to develop new materials with better device performance [1].

The morphology, along with energy level positions of donor and acceptor, influences several aspects that are decisive for achieving high device efficiencies, such as the rate of recombination, the energy required for charge separation and charge mobility.

In this sense, as a means of controlling this property, such as introducing specific additives, post-deposition treatments, or chemical modifications, have motivated research in the synthesis of more ordered, continuous, and more crystalline films [2-4].

In OPV devices, the morphology of the film affects charge transfer at different length scales. For greater orders, the organization of the acceptor and donor domains and the inhomogeneity of crystallinity define the transport mechanisms, in addition to influencing the processes of recombination and separation of charges. On a smaller scale, molecular orientation is also a determining factor [3].

Recently, one of the strategies used to tune the physical, chemical, and electronic properties is by means of the synthesis of terpolymers. These materials consist of three electron acceptor or donor different units associated into the polymer backbone. This approach allows adjusting the material absorption range, the energy level positions and being able to extend the light absorption range in consequence of the appearance of a new π-π* or intramolecular charge transfer (ICT) absorption. Furthermore, it is capable to optimize and balance the effect between solubility and molecular packaging [5].

The polymer microstructure is an essential aspect in the transfer of the charges between the chains and, consequently, in the mobility of the charge transport. Since the morphology of the polymeric films directly influences the charge transport efficiency of optoelectronic devices, the need to evaluate this characteristic of the film is clear. In this context, the union of X-ray absorption spectroscopy and resonant Auger decay spectroscopy presents itself as a useful and straightforward tool for studying the relationship between such properties. The angular dependence of the X-ray absorption spectrum allows obtaining information about the molecular orientation of the polymer chains in relation to the substrate [6-8], whereas the use of the Core-Hole Clock method based on data from the resonant Auger spectroscopy makes it possible to probe the dynamics of charge transfer in the films [9-12]. In this way, it is possible to assess whether new materials and their means of development are promising for a future application in the area of organic optoelectronics.

This work aims to evaluate the preferential molecular orientation of materials with possible application in OPV devices - terpolymer films - based on the dependence of X-ray absorption on the radiation incidence angle. It is also intended to estimate the charge transfer time of the films by the Core-Hole Clock method, pointing out the most promising ones for the intended application. Specifically, for the synthesized terpolymers, it is very interesting to examine the influence of the statistical or block microstructures. We observed that the block terpolymer showed a faster charge transfer dynamics when compared with the statistical terpolymer, indicating itself as a promising candidate in the application in organic solar cell. For this reason, devices based on block terpolymer:$PC_{60}BM$ were produced varying the solvent and the ratio of donor:acceptor.

2. Experimental details

2.1 Materials

Semitransparent metal oxide electrode based on FTO glass was acquired from FlexiTec Electronica Orgânica (Paraná, Brazil) with average sheet resistance ≤5 Ω/sq and used as substrate in the spectroscopic studies. ITO glass (20 Ω / square), PEDOT:PSS (Al4083) was purchased from Ossila, England (5-12 mPas and 500-5000 Ω.cm) and PEDOT:PSS (PH1000) was acquired from Heraeus, Germany (15-60 mPas and 850 S/cm). The terpolymers P5 and P6 were synthesized and reported in another work of Santos and co-workers, 2020 [13]. The terpolymer structures are showed in Table1 and Fig.1.

Table 1

Terpolymer characteristics.

Terpolymer	Monomer Proportion	Copolymer Type
P5	0.5**M1**:**M4**:0.5**M3**	Statistical
P6	(0.5**M1**:0.5**M4**)– (0.5**M3**:0.5**M4**)	Block

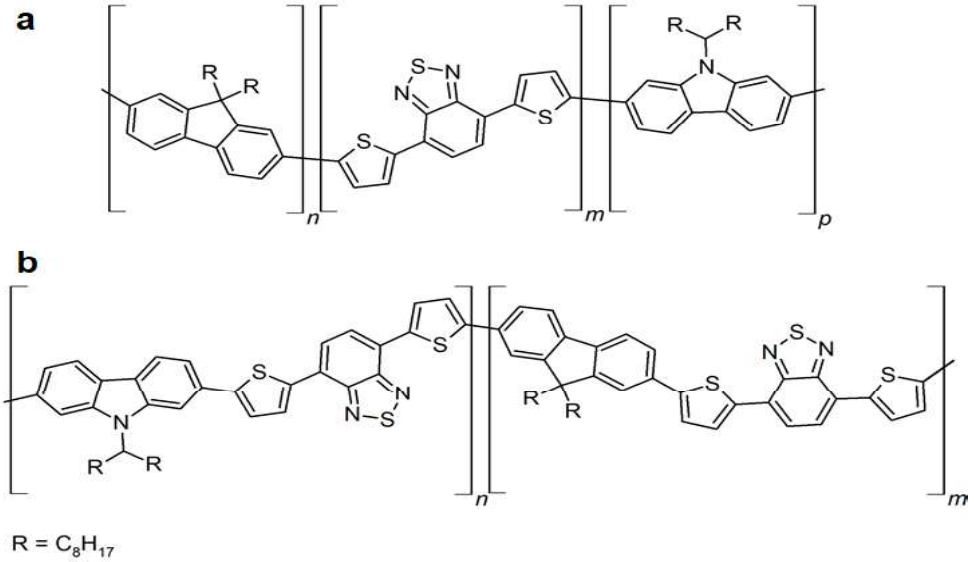

Fig. 1: Structural formula of **(a)** the statistical terpolymer P5 and **(b)** the block terpolymer P6.

2.2 Preparation of terpolymers thin films

FTO substrates were previously cleaned by successive sonication in Hellmanex solution, deionized water, isopropanol, deionized water for 10 min, and dried in N_2. The films were prepared by spin coating on precleaned FTO, using chloroform as solvent (concentration was 0.5 mg/mL). The spin coating was conducted in two stages: 900 rpm/180s and, subsequently, using 1200 rpm/30 s.

2.3 Measurements

2.3.1 X-Ray Absorption Spectroscopy (NEXAFS)

All absorption experiments were carried out in the sulfur K edge region - from 2460 eV to 2495 eV - in the total electron yield detection mode, using Si (111) double-crystal monochromator at the SXS beamline of the Brazilian Synchrotron Light Laboratory (LNLS). Instabilities of the beam flux were corrected by normalization using a gold grid signal placed before the sample. The angular dependence of the NEXAFS spectra was evaluated by rotation of the sample holder mounted perpendicularly to the beam axis to acquire data between 20° (grazing) and 90° (normal) incidence Θ angles. The photon energy scale was calibrated according to polythiophene data reported in the literature [9].

2.3.2 Resonant Auger Spectroscopy (RAS)

For each sample, RAS spectra were obtained for different photon energies representative of relevant regions of the NEXAFS spectrum. Using 20 eV pass energy, data were collected for Auger electrons with kinetic energy between 2100 eV and 2125 eV - sulfur $KL_{2,3}L_{2,3}$ Auger decay range. A linear combination of Gaussian (G) and Lorentzian (L) profile shape functions was used to fit the spectra. The background correction was performed using a Shirley function.

2.3.3 X-ray Photoelectron Spectroscopy (XPS)

XPS measurements were performed using the Thermo Escalab 250 Xi spectrometer, with a monochromatized Al Kα ($h\nu$ = 1486.6 eV) radiation as an X-ray source. The spectrometer's pass energy was 100 eV and 25 eV for the XPS survey and core level spectra measurements, respectively. XPS peak fitting procedures used the software supplied with the spectrometer.

2.3.4 Optical characterization

Time-resolved photoluminescence (TRPL) was measured with an Edinburgh Instruments Lifespec 2 time-correlated single-photon counting operating in reverse mode. The samples were periodically excited with an Edinburgh Instruments EPL405 picoseconds pulsed diode laser ($\lambda_{exc} = 405$ nm, excitation slit width = 5 nm) operating at 20 MHz. The samples emission was measured at $\lambda_{em} = 710$ nm (emission slit width = 20 nm) over a 10 ns time window (512 channels). The TRPL decays obtained were reconvoluted with the instrument response time. Fitting was carried using a single exponential decay:

$$I_{TRPL}(t) \propto e^{-\frac{t}{\tau}}$$

Where τ is the lifetime of excited charge carriers in the fluorophore.

Steady-state photoluminescence was measured with a Horiba Fluoromax-4 fluorometer. The samples emission was measured between 600 and 850 nm ($\lambda_{exc} = 500$ nm, 1 nm step, excitation and emission slit widths = 1 nm). The intensity measured was then normalized concerning the sample absorbance.

Absorbance was measured between 350 and 850 nm with a Perkin Elmer Lambda 9 Ultraviolet-visible spectrophotometer.

2.4 Device Fabrication

After cleaning and drying, the patterned ITO-coated glass substrates were additionally cleaned by oxygen plasma treatment for 20 min at 50°C. PEDOT:PSS (Al4083) was spin-coated on the cleaned ITO glass plates in two stages: 1200 rpm for 10s and, subsequently, using 5000 rpm for 30 s, to give a film thickness of ca. 30 nm. The same conditions were used to deposition the PEDOT:PSS (PH1000) layer, although the viscosity of this HTL is higher. These spin-coated samples were then annealed at 140°C for 10 min on a hot plate. Terpolymers and fullerene derivatives ($PC_{60}BM$ or $PC_{70}BM$) were dissolved (chlorobenzene or dichlorobenzene) together at 70 °C for 180 min. For the active layer preparation with DIO (3% by volume of 1,8-diiodooctane), the DIO additive was added into the polymer/PCBM solution and stirred at 70 °C for 90 min before spin-coating. For the mixture using the statistical terpolymer (P5):PCBM, it was used 15 mg/mL, while for the block terpolymer (P6):PCBM, 20 mg/mL was employed. The solutions were then spin-coated onto the PEDOT:PSS layer at 1000 rpm for 180 s and 1200 rpm for 30 s. For samples with the donor:acceptor ratio 1:2 w/w, three different conditions were used,

500, 800, and 1000 rpm for 240 s followed by 1200 rpm for 30 s. Calcium (40 nm) and aluminum (70 nm) were deposited, under rates of 1 Å/s and 8 Å/s, over the active layer using a thermal evaporator at a base pressure $1x10^{-6}$ Torr. Current density–voltage (J–V) characteristics of devices in dark and under illumination were measured using a programmable Keithley 2400, from -0.1 to 1.10 V for direct scanning, with 10 mV steps and delay time of 0.25 s. The cells were illuminated by AM 1.5 G solar simulator (Solar Science tech class AAA) with reference to a standard Si cell calibrated with NREL at an irradiation intensity of 1000 W/cm^2. The measurements were conducted in the air under ambient conditions.

3. Results

3.1 Spectroscopic studies

The surface chemistry of P5 and P6 films has been characterized by XPS measurements. All core levels emissions expected from the terpolymers – C1s, N1s, S2s, and S2p – were detected in their XPS survey spectra (Fig.2). The presence of O1s core level associated with Si and Sn contributions – the latter only observed for P6 – suggests an uneven polymeric coating of the substrate. Furthermore, oxidative degradation due to air exposure is also a common source of oxygen in organic films [14]. Table 2 lists the atomic percent (at. %) of all elements identified in the survey spectra and also at. % values when not considering elements not originally from the polymers. After the correction, P5 film elemental analysis shows a stoichiometry equivalent to what would be expected based on its chemical structure. P6, on the other hand, has a more relevant deviation from the reference numbers, indicating that this film was possibly more affected by degradation or deposition flaws. Comparing the survey spectra, it is possible to observe clear differences in the background due to secondary low energy electrons. This result, together with the presence of Sn and a higher amount of oxygen for the P6 film, suggests that this film is thinner or less homogeneous than P5.

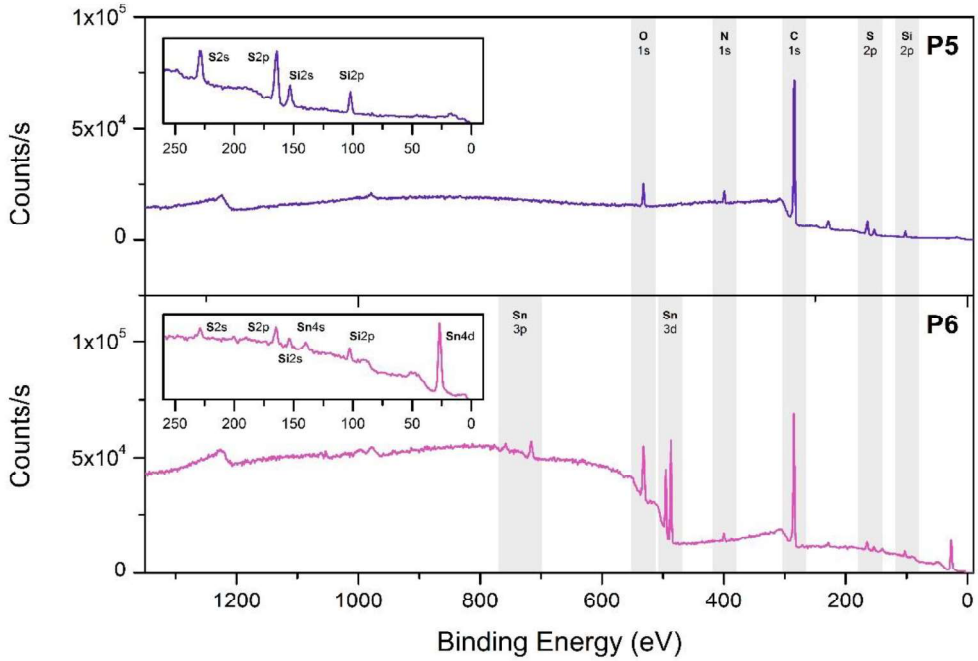

Fig. 2. XPS survey spectra of P5 and P6 terpolymers. Minor emission lines under 250 eV are shown in the insets.

Table 2

Terpolymers elemental analysis according to the XPS survey spectra.

Element	Atomic Percent (%)		Corrected Atomic Percent (%)		Expected Atomic Percent (%)
	P5	P6	P5	P6	
C	81.4	70.7	88.9	91.1	88.7
N	4.4	3.2	4.8	4.2	5.1
S	5.8	3.7	6.3	4.7	6.2
O	5.0	15.6	-	-	-
Si	3.4	2.9	-	-	-
Sn	-	3.9	-	-	-

By analyzing the high-resolution spectra in the C1s, N1s, O1s, and S2p core-level regions presented in Fig. 3, one can notice that most of the features are common to both terpolymers. P5 and P6 are essentially the same polymer in terms of their monomers chemical structure and stoichiometries, differing only by the copolymerization process; therefore, the similarities were indeed expected. It also means that any synthetic differences did not introduce significant undesirable traits.

Among the four main contributions adjusted in the C1s spectra, those at 284.5 eV and 284.9 eV are attributed to sp^2 (C=C) and sp^3-carbons (C-C/C-H), respectively. Table 3 shows the calculated at. % based on the polymers chemical structure, predicting a proportion of 1:0.87 between these two chemical states. However, the experimental data yields a 1:1.16 ratio as a consequence of the smaller amount of C=C contribution fitted. This apparent ratio shift is, presumably, caused by oxidative degradation of the polymeric film surface and adventitious carbon contamination. Since carbon-carbon double bonds are more susceptible to oxidation than the single ones, the low intensity oxidized states fitted (insets in Fig. 3) at higher biding energies can be interpreted mostly as products of such degradation processes, reducing the C=C contribution in the spectrum. Lastly, the following two peaks at 285.4 eV and 286.0 eV are better assigned to C-S and C-N chemical states in the polymers, respectively [15].

Fig. 3: High-resolution XPS spectra at C1s, N1s, O1s, and S2p core levels. Minor contributions over 286 eV in the C1s spectra are shown in the insets.

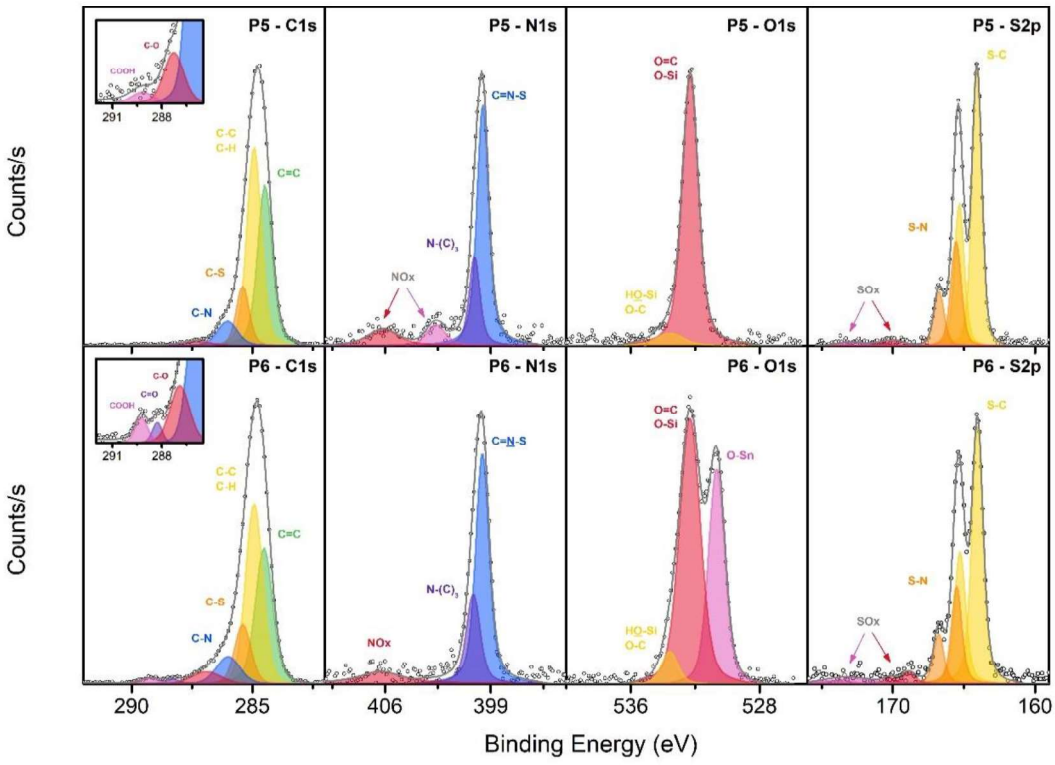

Table 3

Atomic percent of terpolymers chemical states according to high-resolution XPS spectra in C1s, N1s, O1s, and S2p core-level regions. The expected atomic percent based on polymer chemical structures are also presented.

Chemical State	Binding Energy (eV)	Atomic Percent (%)		Expected Atomic Percent (%)
		P5	P6	
C=C	284.5	36.8	33.9	44.2
C-C/C-H	284.9	42.6	39.3	38.4
C-S	285.4	11.2	12.3	9.3
C-N	286.0	7.2	8.2	8.1
C=N-S	399.5	60.5	62.8	80
$N\text{-}(C)_3$	400.1	20.4	25.3	20
O-Sn	530.7	-	36.7	-
O=C/O-Si	532.3	93.1	57.9	-
O-C/HO-Si	533.6	6.9	5.4	-
S-C	164.1(2p3/2)	68.8	68.8	66.7
S-N	165.5 (2p3/2)	27.4	24.2	33.3

Accordingly, the associated nitrogen and sulfur chemical states are found at the N1s and S2p spectra. In the former, an intense peak at 399.5 eV is related to C=N-S in the benzothiadiazole unit [14,16-20] and, appearing as a shoulder, a smaller contribution at 400.1 eV is assigned to $N\text{-}(C)_3$ chemical state from the carbazol units [15,20]. As stated by the atomic percent in Table 3, the amount of C=N-S nitrogen atoms is lower than the terpolymers chemical structure would suggest. Furthermore, once again, minor contributions at higher binding energies were detected, which might be evidence of oxidative degradation of the thiadiazol ring. A similar interpretation can be drawn from the S2p data, where the S-N contribution from benzothiadiazole at 165.5 eV ($2p_{3/2}$) [14,17–19] is also lower than would be expected. Along with possibly SOx states fitted, all these pieces of evidence indicate that the thiadiazol ring is more prone to degradation on the polymeric film surface than other characteristic units. Moreover, the most intense contribution at 164.1 eV ($2p_{3/2}$) is assigned to S-C from the thiophene rings

[14,18,19,21]. Finally, O1s spectra of both terpolymers have peaks around 532.3 eV and 533.6 eV that convolute contributions from chemical states associated with carbon [15] and silicon atoms [22]. Additionally, a third peak can be seen in P6's spectra at 530.7 eV related to tin atoms [22], only perceivable in this film as its survey spectra has demonstrated. Although these features attest to mild levels of oxidative degradation on the film's surface and their non-uniformity, the overall quality of the successfully deposited films was not compromised. Sulfur K-edge NEXAFS spectra of the terpolymers films are shown in Fig. 4. As indicated by their second derivatives, the same four main features (grey-shaded areas) are present in both polymeric films: **f1** centered at 2471.8 eV, **f2** at 2472.8 eV, **f3** at 2473.8 eV, and **f4** at 2475.3 eV. Since P5 and P6 comprise two different units containing sulfur, thiophene (T), and benzothiadiazole (BT), the absorption profile observed can be interpreted as a combination of core-level transitions characteristic of each unit [6,8].

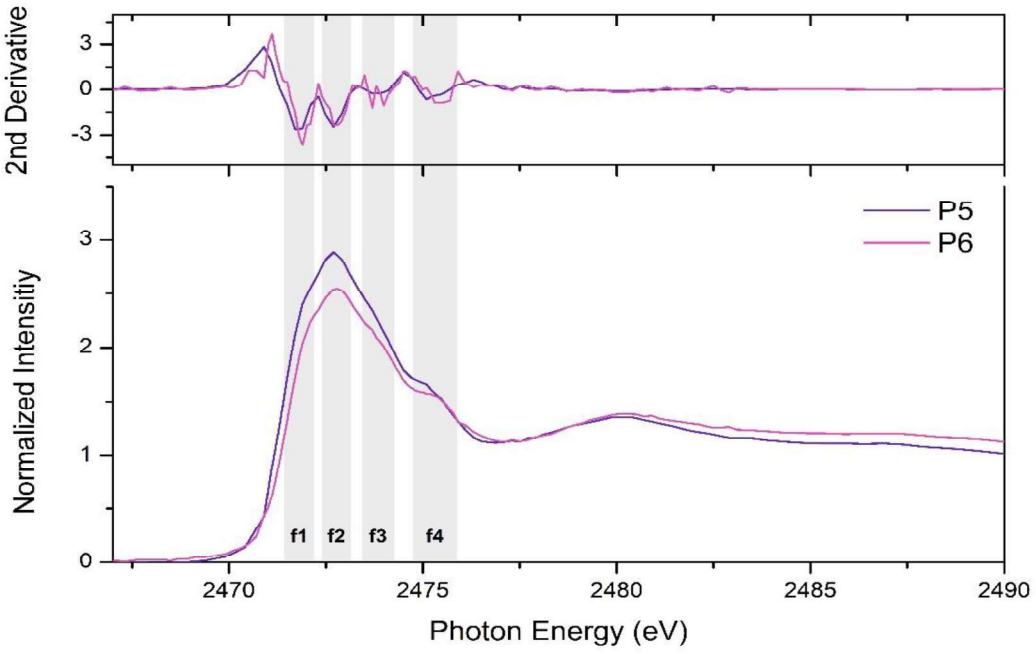

Fig. 4. Sulfur K-edge absorption spectra, and their second derivatives, of P5 and P6 terpolymers recorded at 45° photon incidence. The most four important features (f1, f2, f3 and f4) of both spectra indicated by the second derivatives are highlighted by the gray shaded areas.

Moreover, it might be possible to gather information about T and BT molecular orientation in the terpolymeric films by evaluating the angle dependence of their specific contributions in the spectra.

Based on the poly 3-hexylthiophene (P3HT) absorption spectrum shown in Fig.5a, there are three significant peaks representative of the T unit within the 2470 – 2476 eV photon energy range. The most intense feature of the P3HT spectrum comprises the first two contributions, **t1** and **t2**, which can be assigned to $S1s \rightarrow \pi^*$ and $S1s \rightarrow \sigma^*(S\text{-}C)_{\parallel}$, respectively [23-28]. According to Sekiguchi et al. (2014), [29] the last peak (**t3**) is also related to σ*(S-C) resonance; however, its transition moment is perpendicular to the backbone chain direction ($S1s \rightarrow \sigma^*(S\text{-}C)_{\perp}$), while **t2** has its transition moment parallel to it [29]. All three transitions moments are also mutually orthogonal, as illustrated in Fig.5b.

Concerning the BT unit, Fig.5c shows the sulfur K-edge NEXAFS spectrum of the PFOCBT statistical terpolymer, the analog of P5, but lacking the T units. As reported by its second derivative, three main contributions are noticed within the aforementioned photon energy range of interest. For benzothiadiazole molecule in the gas phase, it is expected two strong peaks spaced 1.7 eV apart, which the least energetic one corresponds to $S1s \rightarrow \pi^*$ transition. In contrast, the second one is related to $S1s \rightarrow \sigma^*(S\text{-}N)$ transition [30]. These assignments are compatible with **b1** and **b2** peaks of the PFOCBT spectrum, respectively. Moreover, a third peak would appear as a shoulder of the second one for the gas phase molecular system, related to a transition to a Rydberg state ($1s \rightarrow 4p$)[30]. At first glance, feature **b3** could be interpreted as equivalent to this peak; however, this type of transition is hardly observed in strongly chemisorbed molecules and condensed systems, such as the polymers films studied here, due to the large size of Rydberg states [6,8].

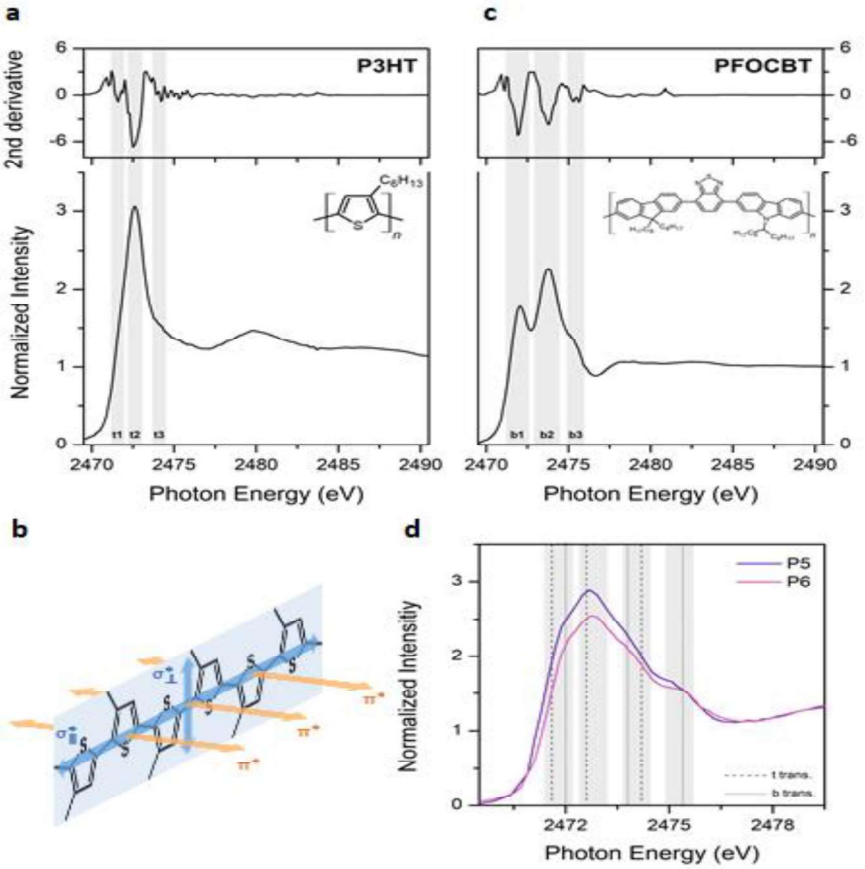

Fig. 5:**(a)** Sulfur K-edge absorption spectrum of P3HT and its second derivative, recorded at 45° photon incidence. Important features (**t1**, **t2,** and **t3**) within the 2470 – 2476 eV photon energy range are highlighted by the gray-shaded areas. **(b)** P3HT transition moment orientations concerning the polymer backbone chain. **(c)** Sulfur K-edge absorption spectrum of PFOCBT and its second derivative were recorded at 45° photon incidence. Significant features (**b1**, **b2,** and **b3**) in the photon energy of interest are also indicated. **(d)** Unit-specific **t** (dashed lines) and **b** (dotted lines) transition contributions expected in P5 and P6 absorption spectra features.

When comparing, in Table 4, the characteristic peaks of T and BT units with those observed in P5 and P6 absorption spectra, it seems that **f1** and **f3** features result, in fact, from the overlapping of two pairs of contributions: **t1**|**b1** and **b2**|**t3**, respectively. Fig.5d demonstrates how these unit-specific transitions are close to each other, suggesting that any sort of dichroism trend

observed for **f1** and **f3** is probably a combination arising from both sulfur-containing units, turning their interpretation a more challenging task.

Table 4

Comparison between P5, P6, T, and BT features.

Energy (eV)	Transition		P5/P6 feature	Energy (eV)
	T	BT		
2471.6	$S1s \rightarrow \pi^*$		**f1**	2471.8
2472.1		$S1s \rightarrow \pi^*$		
2472.6	$S1s \rightarrow \sigma^*(S\text{-}C)_{\parallel}$		**f2**	2472.8
2473.8		$S1s \rightarrow \sigma^*(S\text{-}N)$	**f3**	2473.8
2474.2	$S1s \rightarrow \sigma^*(S\text{-}C)_{\perp}$			
2475.4		**b3**	**f4**	2475.3

The angle dependence of each terpolymer absorption spectrum is displayed in Fig.6. Both samples have evident dichroism, meaning that well-ordered films were formed. In order to better visualize the trends, the intensity difference between the spectra of a giving incident angle and the grazing incidence (20°) spectrum is also presented. Then, it is easy to identify that both terpolymers exhibit basically the same pattern, in which **f1** and **f4** intensities decrease with the increasing angle of incidence, while **f2** and **f3** have the opposite behavior. However, defining a preferred molecular orientation – in respect to the substrate surface – for either T or BT units founded only on these trends is not properly achievable due to the overlapping contributions.

Fig.6: Angle dependence of P5 and P6 terpolymers absorption spectra and their intensity variation regarding the grazing incidence (20°) spectrum. The features energy positions are indicated by gray dotted lines.

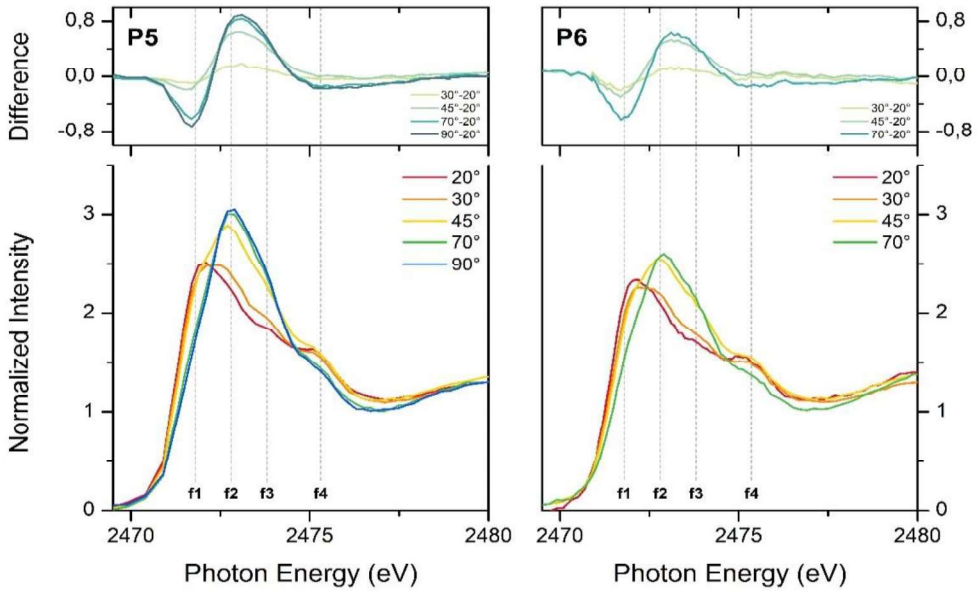

Nevertheless, Density Functional Theory (DFT) calculations of oligomeric systems with the structure containing DTBT as acceptor moiety indicates a dihedral angle between T and BT units' molecular planes, Φ_2 and Φ_3 at Fig.7, lower than 12° [31-33]. These results suggest a condition where they are closer to be parallel to each other (Φ_2, $\Phi_3 \rightarrow$ 0° or 180°) rather than perpendicular (Φ_2, $\Phi_3 \rightarrow$ 90° or 270°). In such a condition, both units must tend to the same configuration with respect to the substrate surface. Furthermore, both transitions comprising the **f1** or **f3** features would exhibit the same dichroism trend, either increasing or decreasing simultaneously with the angle of incidence. Considering that **f1** and **f3** maximum intensities occur at grazing and normal incidence, respectively, the units may be approaching a parallel orientation concerning the substrate surface – also known as a face-on configuration –, given that such conjunction of trends would only be observed when adopting this configuration.

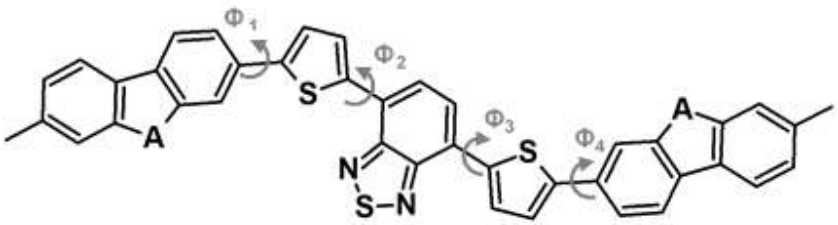

Fig.7: Dihedral angles in P5 and P6 terpolymers.

Charge transfer times (τ_{CT}) of all polymers –P3HT and PFOCBT included for comparative purposes – were estimated by applying the Core-Hole Clock (CHC) method [11,34]. To do so, the resonant (I_{Res}) and normal Auger contributions (I_{NA}) were evaluated by deconvolution of sulfur $KL_{2,3}L_{2,3}$ resonant Auger decay spectra taken at few relevant photon energies according to the NEXAFS spectrum of the polymer. The τ_{CT} corresponding to the resonance maximum in each polymer absorption spectra is listed in Table 5.

Table 5

Polymers charger transfer times at their resonance maximum.

Polymer	τ_{CT} (fs)
P5	9.8
P6	8.5
P3HT	9.2
PFOCBT	49.2

P5 and P6 show τ_{CT} values comparable to P3HT, a widely applied polymer in photovoltaic devices, suggesting that these new polymers might be promising materials in such applications. Among both terpolymers, the block copolymer type P6 has a considerably faster charge transfer dynamic than its statistical copolymer analog and slightly faster than P3HT. This result indicates that the type of copolymer plays an important role in the terpolymer electronic properties, despite not having the same impact on its molecular orientation.

PFOCBT, on the other hand, has a high τ_{CT} as a consequence of a low normal Auger (NA) contribution in its RAS spectrum, as demonstrated in Fig.8. Such evidence implies a low charge transfer rate when BT is not associated with T units. Incorporating the latter leads to a substantial increase in the terpolymer charge-transfer capabilities, possibly improving their performance as part of the active layer in BHJ solar cells. According to DFT calculations performed by Damas et al. (2018), [33] a significant reduction of the torsional angles is observed when BT is replaced by DTBT in similar oligomeric systems [33]. The resulting increase in the polymer backbone planarity – and consequently, better electron delocalization – caused by the T units addition provides a more efficient charge transfer.

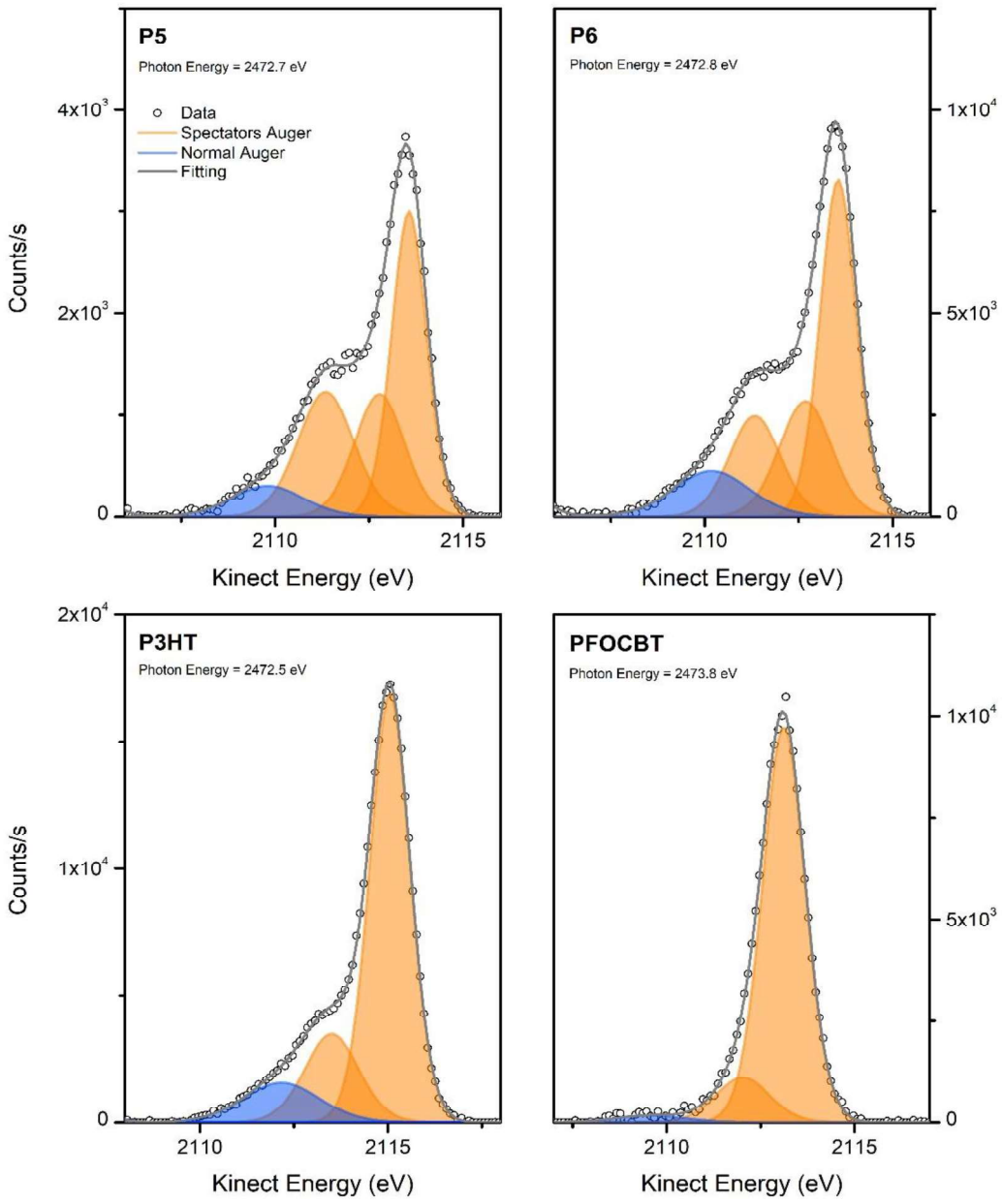

Fig. 8: Sulfur $KL_{2,3}L_{2,3}$ resonant Auger decay spectra of polymers at their maximum resonance intensity. Normal Auger contributions are depicted as blue and spectators Auger contributions as orange.

3.2 Optical properties of the polymer thin-films

Steady-state and time-resolved photoluminescence measurements were made of the neat polymer films. As expected, both polymers have similar absorbance and emission spectra shapes; however, P6 was found to have a significantly higher absorbance and emission intensity (Fig. 9). The PL intensity of P6 was >2 fold higher than that of P5 under the same excitation conditions and normalized to the differences in absorbance. Furthermore, the photoluminescence lifetime of P6 was found to be slightly shorter than that of P5, suggesting that the rate of radioactive recombination for P6 is greater than that of P5 (Fig. 9b). However, both polymers show a fairly short radioactive lifetime. A higher rate of radioactive recombination, coupled with higher photoluminescence intensity, in these neat films is desirable, as it is an indicator of the potential excited state electrons that can possibly be extracted as current in a full device. It would suggest that P6 has the potential to generate more photocurrent in a full device but that both are promising for device application. Furthermore, the transmission of the films (from absorbance measurements) at 500 nm is 25% and 5% for P5 and P6 respectively, this is expected as both films are opaque in nature, but the higher light absorption from P6 indicates it has better potential for light-harvesting in this range. Given that the charge transfer times for P6 are also slightly faster than P5 (Table 5), one would expect P6 to be the better performing polymer in full devices.

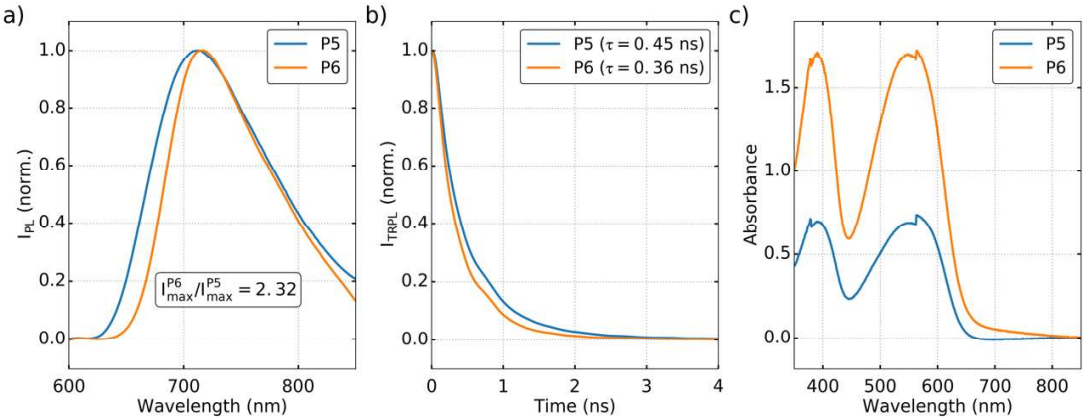

Fig. 9: Optical properties of thin-film samples of P5 and P6; (a) normalized steady-state photoluminescence spectra and intensity ratio (excitation wavelength of 500 nm and excitation/emission slits of 1 nm), (b) time-resolved fluorescence decays and associated lifetimes measured with a picosecond diode laser operating at 20 MHz (excitation wavelength = 405 nm,

excitation and emission slit widths of 5 and 20 nm respectively) and (c) absorbance spectra between 350 – 850 nm.

3.3 Photovoltaic Properties

In order to investigate the performance of the active layers, terpolymers were paired with $PC_{60}BM$ or $PC_{70}BM$ to fabricate the devices using the conventional architecture of ITO/PEDOT:PSS/Active Layer/Ca/Al (Fig. 10).

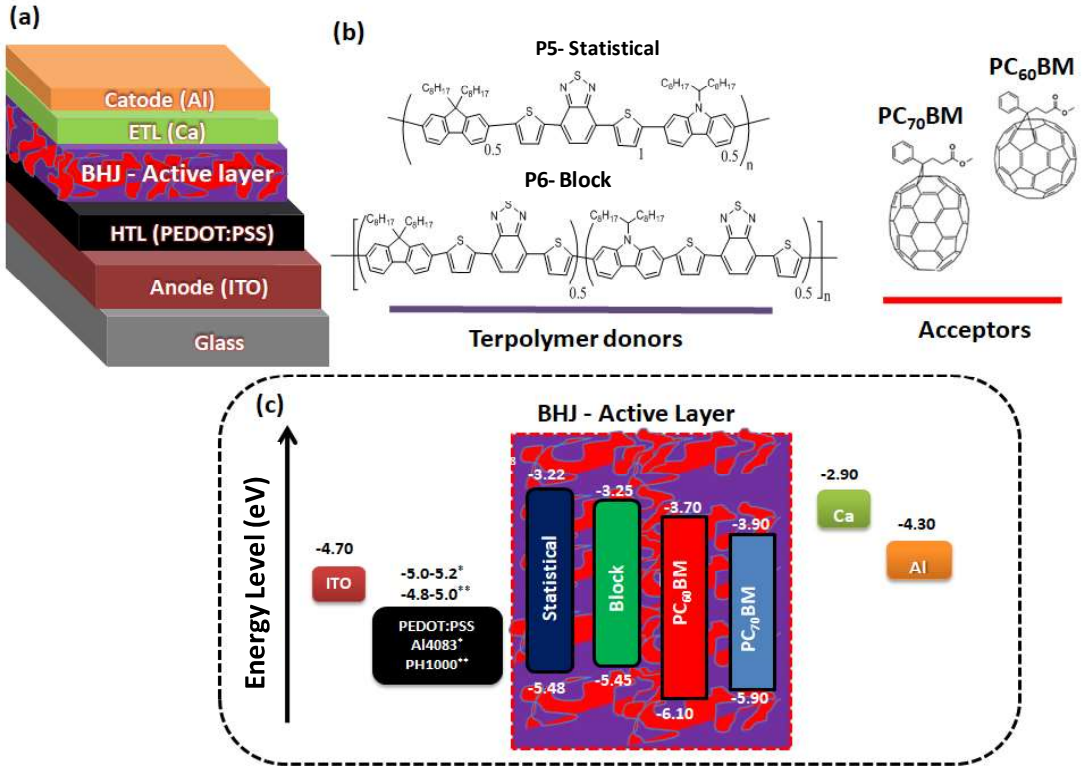

Fig. 10: Device structure of all-OPV (a). Chemical structures of the polymer donors and acceptors used in this study (b). Energy-level diagram of conventional configuration (c).

Fig. 11 and 12 show the current density-voltage (J-V) curves of these devices employing donor P5. The summary of the device performance parameters for the active layers based on terpolymer:acceptor is listed in Table 6.

Mola and Abela (2014) [35] point out that LUMO offset (ΔE_{LL}) measured from the difference between the LUMO levels of donor and acceptor of at least 0.3 eV is enough to dissociate the photo-generated exciton in the active layer. Therefore, both terpolymers showed ΔE_{LL} above this condition (Fig. 10c).

Initially, all photovoltaic cells based on the device structure of ITO/PEDOT:PSS(Al4083)/P5:Acceptor/Ca/Al showed an open-circuit voltage higher than 0.8 V. According to Blakesley and Neher (2011), [36] V_{oc} depends essentially on balance between charge carrier generation and recombination in the active region. Kim et al. (2016) [37] synthesized PFDTBT, a polymer composed of fluorene, thiophene, and benzothiadiazole monomers, where the authors obtained V_{oc} of 0.92 V employing this donor combined with $PC_{70}BM$ in BHJ solar cell. The maximum power conversion efficiency (PCE) of 1.5% and a short-circuit current of 4.03 mA/cm² was obtained in the device employing P5:$PC_{60}BM$ (after annealing at 95°C). It may be due to the energy levels between the terpolymer and this acceptor, as can be observed in Fig. 10c, which indicates better energy level alignment with $PC_{60}BM$.

The thermal annealing treatment has the objective of rearranging and enhancing the active layer morphology. Both terpolymers do not present a significant degree of chain ordering, and T_g was not observed in DSC analysis (**Supporting information**). We believe that the polymer T_g is above the performed thermal treatment. Therefore, if the annealing was conducted at a higher temperature than Tg, the PCE could be increased due to increased phase separation. Furthermore, we suppose that this occurs due to the presence of carbazole in the conjugated polymer chain, which generates rigidity in the chain, thus making packaging difficult. Some works reported in the literature did not observe transitions by DSC. Guo and co-workers (2016) [38] synthesized a series of D1-A-D2-A thermocouples based on diketopyrrolpyrrole (DPP) as an acceptor unit (A), benzothiophene substituted with alkylthienyl (BDTT) and 2,5-bis (2-alkyloxylbenzene thiophene) (TBT) as electron donors (D1 and D2). No transition was observed in the DSC, ranging from 40-300 °C in the proposed polymers due to the chains' rigidity.

The other strategy employed in BHJ-solar cells is the addition of solvent additives as diiodoctane with the purpose to change the morphology of the active layer, reduce the phase segregation and increase the solubility between polymer and fullerene derivative. As shown in Fig.11 and Table 6, J_{sc} and PCE increased in the device where diiodoctane was used compared to the same active layer (P5:$PC_{70}BM$). The additive acts to reduce the size of fullerene derivative clusters, then the aggregates of acceptor dissolve and a higher interface area between polymer chain and fullerene molecules are formed.

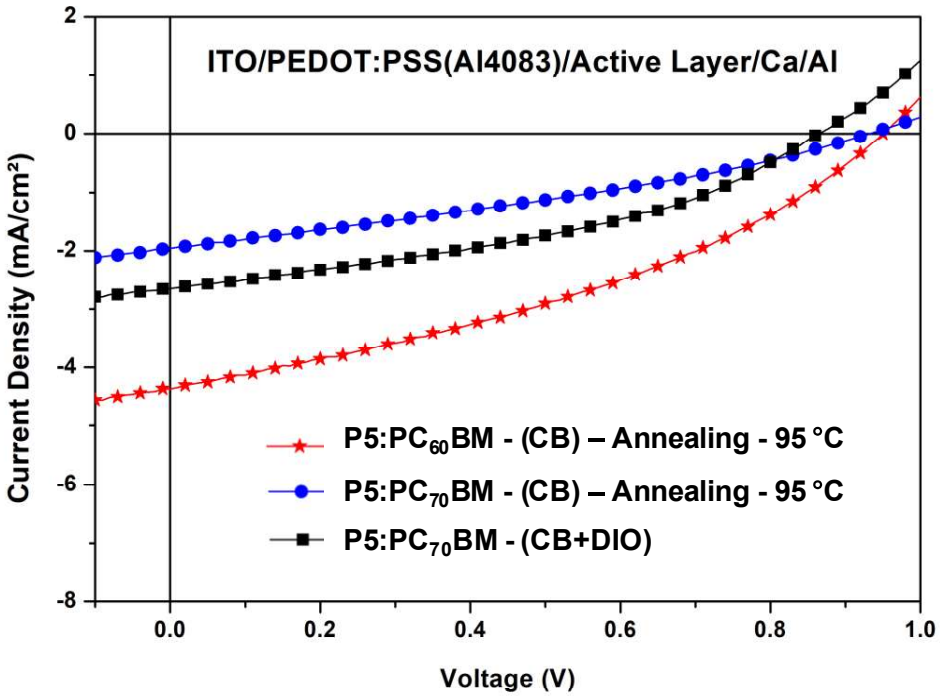

Fig. 11: Current density–voltage (J-V) curves under illumination of organic solar cells of ITO/PEDOT:PSS (Al4083)/Active Layer/Ca/Al devices with an active layer D/A of 1:1 w/w in chlorobenzene.

Moreover, the device based on statistical terpolymer:$PC_{60}BM$ and HTL-PH1000 showed the highest PCE value of 1.2% (Fig.12). The DIO added to the active layer increased the J_{sc} from 1.9 to 3.6 mA/cm² when compared to the same acceptor without additive, and PCE of 1.11% was obtained.

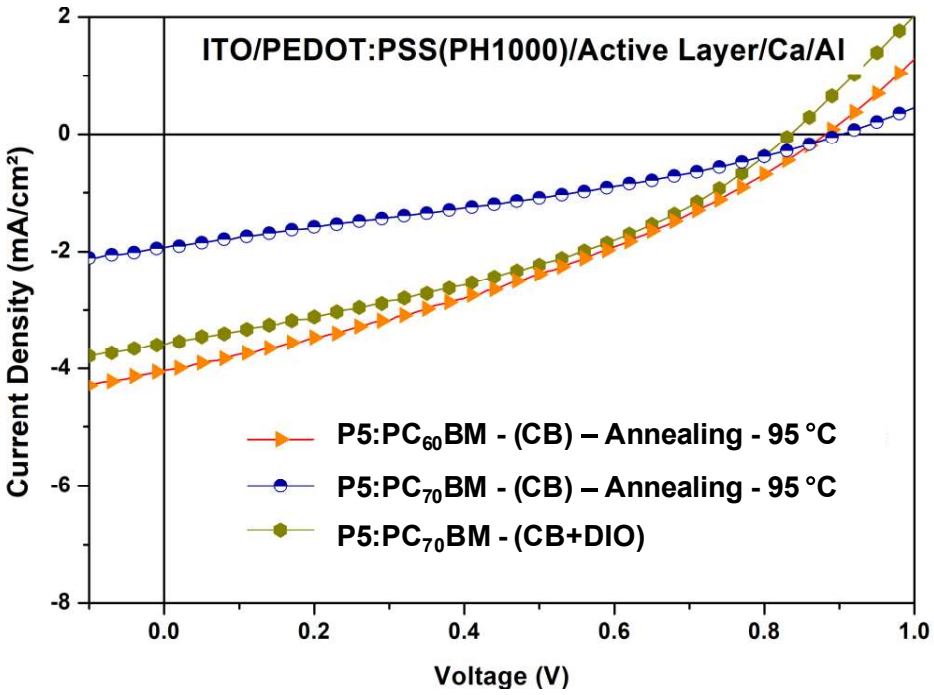

Fig. 12: Current density–voltage (J-V) curves under illumination of organic solar cells of ITO/PEDOT:PSS (PH1000)/Active Layer/Ca/Al devices with an active layer D/A of 1:1 w/w in chlorobenzene.

Table 6

Photovoltaic Performance of the Statistical and Block Terpolymers.

Donor	Acceptor	Ratio/Solvent/ HTL	Annealing (°C)	V_{oc} (V)	J_{sc} (mA/cm²)	FF (%)	PCE (%)
P5	$PC_{70}BM$	1:1/CB/Al4083	95	0.95	2.00	40	0.74
	$PC_{70}BM$	1:1/CB+DIO/Al4083	----	0.86	2.60	39	0.88
	$PC_{60}BM$	1:1/CB/Al4083	95	0.95	4.40	36	1.50
	$PC_{70}BM$	1:1/CB/PH1000	95	0.91	1.90	37	0.64
	$PC_{70}BM$	1:1/CB+DIO/PH1000	----	0.84	3.60	37	1.11
	$PC_{60}BM$	1:1/CB/PH1000	95	0.89	4.05	34	1.20
P6	$PC_{70}BM$	1:1/CB/Al4083	95	0.92	2.20	29	0.60
	$PC_{60}BM$	1:1/CB+DIO/Al4083	----	0.86	4.10	32	1.00
	$PC_{60}BM$	1:1/CB/Al4083	95	0.86	3.40	32	0.90
	$PC_{70}BM$	1:1/CB/PH1000	95	0.90	3.40	29	0.90
	$PC_{60}BM$	1:1/CB+DIO/PH1000	----	0.86	4.70	34	1.40
	$PC_{60}BM$	1:1/CB/PH1000	95	0.86	4.10	30	1.10

Fig.13 presents the current density–voltage (J-V) curves for the device mounted with P6:acceptor and HLT (Al4083). The devices using thermal annealing and active layer with $PC_{60}BM$ showed the highest photovoltaic parameters, short-circuit current (J_{sc}) of 3.40 mA/cm^2, open-circuit voltage (V_{oc}) of 0.86 V, and fill-factor (FF) of 32% under the solar simulator, giving a power conversion efficiency (PCE) of 0.9%. Employing the DIO additive in the same configuration resulted in a improve the Jsc of all devices significantly with a slight loss in V_{oc}, indicating the influence of this additive in organic solar cells, improving the dispersion of the fullerene derivative.

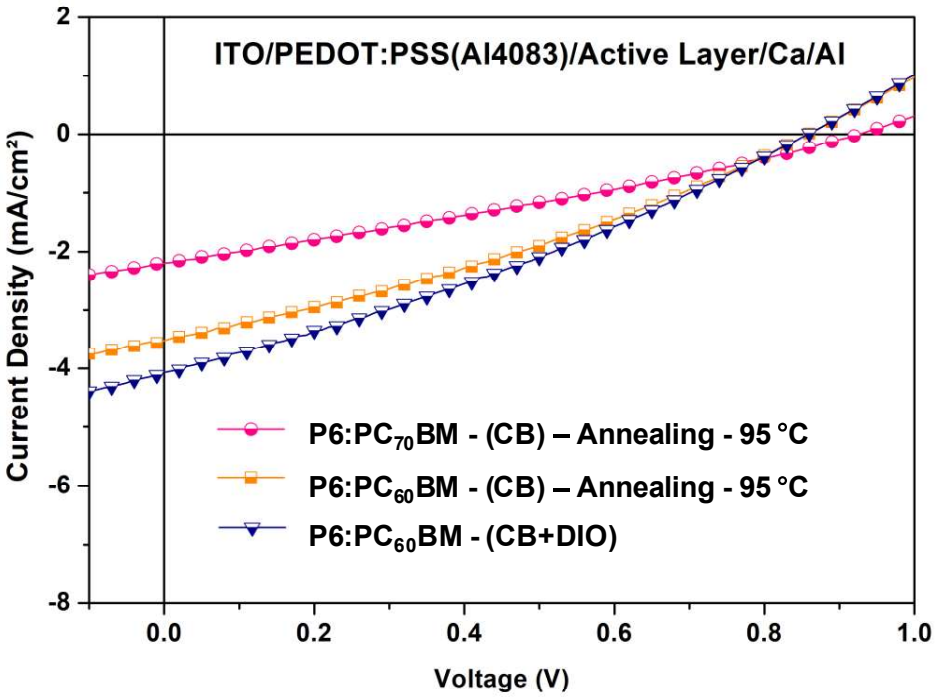

Fig.13: Current density–voltage (J-V) curves under illumination of organic solar cells of ITO/PEDOT:PSS (Al4083)/Active Layer/Ca/Al devices with an active layer D/A of 1:1 w/w in chlorobenzene.

We verified that the type of PEDOT:PSS used affected the efficiency mainly due to the high conductivity of PH1000 [39,40]. The best performance regarding the use of the block terpolymer as the donor was obtained when DIO and HTL-PH1000 were used in the device, with a short-circuit current (J_{sc}) of 4.70 mA/cm² and a fill factor (FF) of 34%, leading to a PCE of 1.4% (Fig. 14).

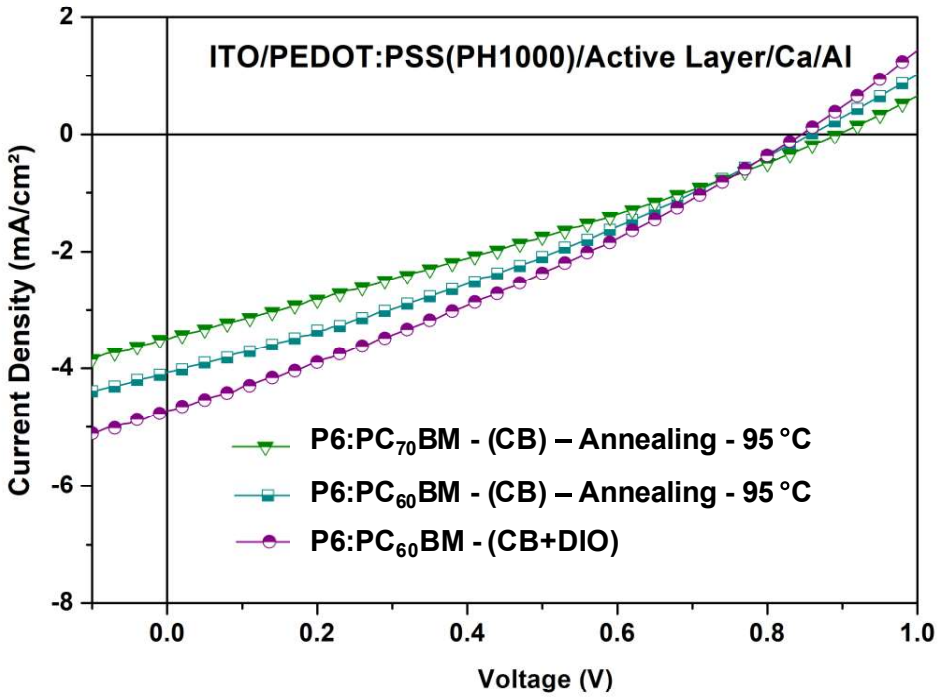

Fig. 14: Current density–voltage (J-V) curves under illumination of organic solar cells of ITO/PEDOT:PSS (PH1000)/Active Layer/Ca/Al devices with an active layer D/A of 1:1 w/w in chlorobenzene.

After that, devices were produced applying block terpolymer (P6) using O-DCB, adding 1,8-diiodooctane (DIO) additive, and changing the rotation of the spin coating for the deposition of 500, 800, and 1000 rpm (Fig.15***Fig.*** and Table 7). According to Guo et al. 2016 [41], this additive can enhance the photovoltaic performance of the active layer by improving interpenetrating nanoscale morphologies. The P6:$PC_{60}BM$ weight ratio was optimized from 1:2(1000, 800, and 500 rpm) and 1:1 (1000rpm). The device fabricated from the blend solutions with a P6:$PC_{60}BM$ weight ratio of 1:2 (1000rpm) shows a PCE of 0.3% with a J_{sc} of 2.19 mA/cm^2, a V_{oc} of 0.44V, and a fill factor (FF) of 33%. Reducing the spin-coating speed generally increased the PCEs with 800 rpm>500 rpm >1000 rpm. The device containing the 1:2 w/w blend ratio and 800 rpm as the photoactive layer has superior performance, with a 1.2% PCE. We believe that with a higher amount of electron acceptor, even deposited at low speed, an

active layer with a small thickness was obtained. Furthermore, we observed that when the solvent dichlorobenzene was used, the solubility increased.

Additionally, we fabricated a similar device, as reported by Santos et al., 2020 [13]. The difference was that the photovoltaic measurements were carried out in the air. The device ITO/PEDOT:PSS(Al4083)/Block:$PC_{60}BM$(1:1+DCB+CB)/Ca/Al had a PCE of ca. 2.2%. We observed mainly two differences between the devices relative to the photovoltaic parameters. The first was the increase in V_{oc}, and the second was related to lower J_{sc} compared to those reported by Santos and co-workers (2020) [13]. These results corroborate those obtained by Ceballos and co-workers in 2015 [42]. In the air, the hydration of the PEDOT:PSS may occur, increasing its work function. Instead, the decrease of J_{sc} can be explained by a reduction in charge-carrier, and the generation of trap states mobility when the device is exposed to air and light. Despite this difference, a similar PCE was obtained.

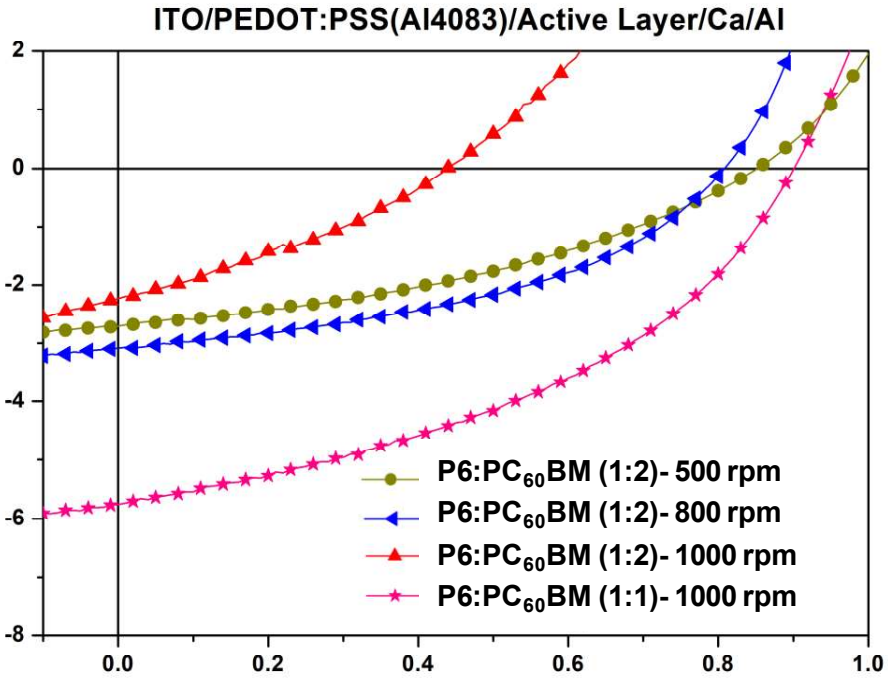

Fig. 15: Current density–voltage (J-V) curves under illumination of organic solar cells of ITO/PEDOT:PSS (Al4083)/P6:PC60BM/Ca/Al devices with an active layer D/A 1:2 and 1:1 w/w in the o-dichlorobenzene+additive and different rotation of spin coating.

Table 7

Photovoltaic Performance of the P6:$PC_{60}BM$.

Donor	Acceptor	Ratio/Solvent/ HTL/rotation	V_{oc} (V)	J_{sc} (mA/cm²)	FF (%)	PCE (%)
P6	$PC_{60}BM$	1:2/DCB+DIO/ Al4083-1000rpm	0.44	2.20	33	0.35
	$PC_{60}BM$	1:2/DCB+DIO/ Al4083-800rpm	0.81	3.15	47	1.18
	$PC_{60}BM$	1:2/DCB+DIO/ Al4083-500rpm	0.85	2.70	42	1.00
	$PC_{60}BM$	1:1/DCB+DIO/ Al4083-1000rpm	0.91	5.73	42	2.20

4. Conclusions

P5 and P6 terpolymers were properly synthesized and deposited over the FTO substrate, as shown by XPS surface characterization. However, both films are not evenly covering the substrate, and the block polymer (P6) seems to be thinner and more affected by degradation. Although the dichroism analysis of their NEXAFS spectra indicates well-ordered films in both cases, the average orientation of the sulfur-containing units is not clear. A common face-on orientation of T and BT units is plausible, and further analysis should be considered to attest to such configuration. According to the charge transfer times estimated by the CHC method applied to RAS measurements, P6 has faster charge transfer dynamics than its statistical analog (P5) and P3HT. By comparing with PFOCBT, we were also able to observe the positive impact of introducing thiophene units between donor and acceptor moieties on the charge transfer dynamics of such semiconducting polymers.

Furthermore, P6 seems to have better optical properties than P5 with improved light absorption in a thin film, a greater degree of photoluminescence (ca. 2 fold higher than P5 normalized to absorbance), and a shorter fluorescence lifetime all indicating a greater potential for charge generation in full devices. Then, BHJ solar cells were fabricated with both donor polymers (P5 and P6). We found that the $PC_{60}BM$ showed higher photovoltaic parameters in both materials than employing $PC_{70}BM$, and generally, P6 performs better than P5. By adding DIO, it was verified a significant increase in J_{sc} and PCE. Also, the type of solvent provided a powerful route for optimizing the device preparation and maximizing the performance of organic electronic devices. Moreover, the devices using a higher ratio of PCBM to polymer and faster spin coating rotation showed different results, highlighting the speed of 800 rpm, obtaining 1.18% of PCE. Furthermore, the best performance of the OPV devices was obtained for the block terpolymer P6:$PC_{60}BM$ (PCE = 2.2%), producing an optimized active layer.

References

[1] G. Nagarjuna, D. Venkataraman, Strategies for controlling the active layer morphologies in OPVs, Journal of Polymer Science Part B: Polymer Physics. 50 (2012) 1045–1056. https://doi.org/10.1002/polb.23073.

[2] W. Cao, J. Xue, Recent progress in organic photovoltaics: Device architecture and optical design, Energy and Environmental Science. 7 (2014) 2123–2144. https://doi.org/10.1039/c4ee00260a.

[3] W. Chen, M.P. Nikiforov, S.B. Darling, Morphology characterization in organic and hybrid solar cells, Energy and Environmental Science. 5 (2012) 8045–8074. https://doi.org/10.1039/c2ee22056c.

[4] C. Wang, H. Dong, W. Hu, Y. Liu, D. Zhu, Semiconducting π-Conjugated Systems in Field-Effect Transistors, Chemical Reviews. 112 (2012) 2208–2267. https://doi.org/10.1021/cr100380z.

[5] T.E. Kang, K.-H. Kim, B.J. Kim, Design of terpolymers as electron donors for highly efficient polymer solar cells, Journal of Materials Chemistry A. 2 (2014) 15252. https://doi.org/10.1039/C4TA02426E.

[6] G. Hähner, Near edge X-ray absorption fine structure spectroscopy as a tool to probe electronic and structural properties of thin organic films and liquids, Chemical Society Reviews. 35 (2006) 1244–1255. https://doi.org/10.1039/b509853j.

[7] M.M. Nahid, E. Gann, L. Thomsen, C.R. McNeill, NEXAFS spectroscopy of conjugated polymers, European Polymer Journal. 81 (2016) 532–554. https://doi.org/10.1016/j.eurpolymj.2016.01.017.

[8] Stöhr, J. NEXAFS spectroscopy. [s.l.] Springer-Verlag Berlin Heidelberg, **1992**.

[9] C. Arantes, B.G.A.L. Borges, B. Beck, L.S. Roman, M. Luiza, M. Rocco, Femtosecond Electron Delocalization in Poly (thiophene) Probed by Resonant Auger Spectroscopy Femtosecond Electron Delocalization in Poly (thiophene) Probed by Ultrafast electron dynamics in the low-femtosecond regime was evaluated for, Journal of Physical Chemistry. (2013) 8208–8213.

[10] Y. Garcia-Basabe, B.G.A.L. Borges, D.C. Silva, A.G. Macedo, L. Micaroni, L.S. Roman, M.L.M. Rocco, The interplay of electronic structure, molecular orientation and charge transport in organic semiconductors: Poly(thiophene) and poly(bithiophene),

Organic Electronics. 14 (2013) 2980–2986. https://doi.org/10.1016/j.orgel.2013.08.022.

[11] L. Cao, X.Y. Gao, A.T.S. Wee, D.C. Qi, Quantitative femtosecond charge transfer dynamics at organic/electrode interfaces studied by core-hole clock spectroscopy, Advanced Materials. 26 (2014) 7880–7888. https://doi.org/10.1002/adma.201305414.

[12] R. Friedlein, S. Braun, M.P. De Jong, W. Osikowicz, M. Fahlman, W.R. Salaneck, Ultra-fast charge transfer in organic electronic materials and at hybrid interfaces studied using the core-hole clock technique, Journal of Electron Spectroscopy and Related Phenomena. 183 (2011) 101–106. https://doi.org/10.1016/j.elspec.2010.11.001.

[13] B. P. S Santos, A. B. Lima, F. L. Araújo, I. C. Mota, A. C. Ribeiro, A. F. Nogueira, J. G. M. Furtado, M. F.V. Marques, F. C. G. Filho, S. N. Monteiro. Synthesis of novel low bandgap random and block terpolymers with improved performance in organic solar cells. (Submitted)

[14] J. Kettle, H. Waters, Z. Ding, M. Horie, G.C. Smith, Chemical changes in PCPDTBT:PCBM solar cells using XPS and TOF-SIMS and use of inverted device structure for improving lifetime performance, Solar Energy Materials and Solar Cells. 141 (2015) 139–147. https://doi.org/10.1016/j.solmat.2015.05.016.

[15] Beamson, G. Briggs, D. High Resolution XPS of Organic Polymers; John Wiley & Sons Ltd: Chichester, **1992**.

[16] B.G.A.L. Borges, C.F.N. Marchiori, M. Glaser, Y. Garcia-Basabe, C.E.V. de Moura, A.B. Rocha, L.S. Roman, T. Chassé, M.B. Casu, M.L.M. Rocco, Electronic and structural properties in thermally annealed PSiF-DBT:PC71BM blends for organic photovoltaics, Thin Solid Films. 615 (2016) 165–170. https://doi.org/10.1016/j.tsf.2016.07.012.

[17] B.G.A.L. Borges, A.G. Veiga, M. Gioti, A. Laskarakis, L. Tzounis, S. Logothetidis, M.L.M. Rocco, Surface, interface and electronic properties of F8:F8BT polymeric thin films used for organic light-emitting diode applications, Polymer International. 67 (2018) 691–699. https://doi.org/10.1002/pi.5552.

[18] M. Gora, W. Krzywiec, J. Mieczkowski, E.C. Rodrigues Maia, G. Louarn, M. Zagorska, A. Pron, Alternating copolymers of diketopyrrolopyrrole or benzothiadiazole and alkoxy-substituted oligothiophenes: Spectroscopic, electrochemical and

spectroelectrochemical investigations, Electrochimica Acta. 144 (2014) 211–220. https://doi.org/10.1016/j.electacta.2014.07.147.

[19] H. Hintz, H. Peisert, U. Aygül, F. Latteyer, I. Biswas, P. Nagel, M. Merz, S. Schuppler, D. Breusov, S. Allard, U. Scherf, T. Chassé, Electronic structure and interface properties of a model molecule for organic solar cells, ChemPhysChem. 11 (2010) 269–275. https://doi.org/10.1002/cphc.200900626.

[20] S. Cho, J.H. Seo, S.H. Park, S. Beaupré, M. Leclerc, A.J. Heeger, A thermally stable semiconducting polymer, Advanced Materials. 22 (2010) 1253–1257. https://doi.org/10.1002/adma.200903420.

[21] B.P. Silva Santos, J.J. Rubio Arias, L.S. Albuquerque, A.G. da Veiga, J.G. de Melo Furtado, A. de Castro Ribeiro, L.A.F. da Silva, E.V. Bendinelli, M.L.M. Rocco, R. Valaski, M. de F. Vieira Marques, An investigation on the effect of the monomer/catalyst ratio in the electronic properties of poly(3-hexylthiophene) using XPS, REELS and UPS techniques, Journal of Electron Spectroscopy and Related Phenomena. 234 (2019) 27–33. https://doi.org/10.1016/j.elspec.2019.05.008.

[22] A. V Naumkin, A.Kraut-Vass, S. W.Gaarenstroom, C. J. Powell. NIST X-ray Photoelectron Spectroscopy Database, NIST Standard Reference Database 20, Version 4.1 http://srdata.nist.gov/xps/.

[23] A.P. Hitchcock, J.A. Horsley, J. Stöhr, Inner shell excitation of thiophene and thiolane: Gas, solid, and monolayer states, The Journal of Chemical Physics. 85 (1986) 4835–4848. https://doi.org/10.1063/1.451718.

[24] M. Kiguchi, G. Yoshikawa, K. Saiki, Temperature and thickness dependence of molecular orientation of α-sexithienyl on Cu(111), Journal of Applied Physics. 94 (2003) 4866–4870. https://doi.org/10.1063/1.1609637.

[25] M. Kiguchi, S. Entani, K. Saiki, G. Yoshikawa, One-dimensional ordered structure of α-sexithienyl on Cu(110), Applied Physics Letters. 84 (2004) 3444–3446. https://doi.org/10.1063/1.1736315.

[26] G. Yoshikawa, M. Kiguchi, S. Ikeda, K. Saiki, Molecular orientations and adsorption structures of α-sexithienyl thin films grown on Ag (1 1 0) and Ag (1 1 1) surfaces, Surface Science. 559 (2004) 77–84. https://doi.org/10.1016/j.susc.2004.04.045.

[27] R. Onoki, G. Yoshikawa, Y. Tsuruma, S. Ikeda, K. Saiki, K. Ueno, Nanotransfer

of the polythiophene molecular alignment onto the step-bunched vicinal si(111) substrate, Langmuir. 24 (2008) 11605–11610. https://doi.org/10.1021/la8016722.

[28] S. Behyan, Y. Hu, S.G. Urquhart, Sulfur 1s near edge x-ray absorption fine structure spectroscopy of thiophenic and aromatic thioether compounds, Journal of Chemical Physics. 138 (2013) 1–12. https://doi.org/10.1063/1.4807604.

[29] Ikeura-Sekiguchi, H.; Sekiguchi, T. Molecular ordering effect of regioregular poly(3-hexylthiophene) using sulfur K-edge X-ray absorption spectroscopy. Jpn. J. Appl. Phys. 2014, *53,* 02BB07-1-4.

[30] A.P. Hitchcock, R.S. DeWitte, J.M. Van Esbroeck, P. Aebi, C.L. Frenc, R.T. Oakley, N.P.C. Westwood, A valence- and inner-shell electronic and photoelectron spectroscopic study of the frontier orbitals of 2,1,3-benzothiadiazole, C6H4SN2, 1,3,2,4-benzodithiadiazine, C6H4S2N2, and 1,3,5,2,4-benzotrithiadiazepine, C6H4S3N2, Journal of Electron Spectroscopy and Related Phenomena. 57 (1991) 165–187. https://doi.org/10.1016/0368-2048(91)85021-K.

[31] L. Pandey, C. Risko, J.E. Norton, J.L. Brédas, Donor-acceptor copolymers of relevance for organic photovoltaics: A theoretical investigation of the impact of chemical structure modifications on the electronic and optical properties, Macromolecules. 45 (2012) 6405–6414. https://doi.org/10.1021/ma301164e.

[32] X. Wang, H. Wang, Y. Yang, Y. He, L. Zhang, Y. Li, X. Li, Zinc tetraphenylporphyrin-fluorene branched copolymers: Synthesis and light-emitting properties, Macromolecules. 43 (2010) 709–715. https://doi.org/10.1021/ma9023119.

[33] G. Damas, C.F.N. Marchiori, C.M. Araujo, On the Design of Donor-Acceptor Conjugated Polymers for Photocatalytic Hydrogen Evolution Reaction: First-Principles Theory-Based Assessment, Journal of Physical Chemistry C. 122 (2018) 26876–26888. https://doi.org/10.1021/acs.jpcc.8b09408.

[34] D. Menzel, Ultrafast charge transfer at surfaces accessed by core electron spectroscopies, Chemical Society Reviews. 37 (2008) 2212–2223. https://doi.org/10.1039/b719546j.

[35] G.T. Mola, N. Abera, Correlation between LUMO offset of donor/acceptor molecules to an open circuit voltage in bulk heterojunction solar cell, Physica B: Condensed Matter. 445 (2014) 56–59. https://doi.org/10.1016/j.physb.2014.04.004.

[36] J.C. Blakesley, D. Neher, Relationship between energetic disorder and open-circuit voltage in bulk heterojunction organic solar cells, Physical Review B - Condensed Matter and Materials Physics. 84 (2011). https://doi.org/10.1103/PhysRevB.84.075210.

[37] H. Kim, H. Lee, Y. Jeong, J.U. Park, D. Seo, H. Heo, D. Lee, Y. Ahn, Y. Lee, Donor-acceptor polymers with a regioregularly incorporated thieno[3,4-b]thiophene segment as a π-bridge for organic photovoltaic devices, Synthetic Metals. 211 (2016) 75–83. https://doi.org/10.1016/j.synthmet.2015.11.016.

[38] X. Guo, M. Zhang, W. Ma, S. Zhang, J. Hou, Y. Li, Effect of solvent additive on active layer morphologies and photovoltaic performance of polymer solar cells based on PBDTTT-C-T / PC71BM, RSC Advances. 6 (2016) 51924–51931. https://doi.org/10.1039/c6ra06020j.

[39] C. Ph, Signi fi cant Di ff erent Conductivities of the Two Grades of Poly(3,4-ethylenedioxythiophene):Poly(styrenesulfonate), Clevios P and Clevios PH1000, Arising from Di ff erent Molecular Weights, (2012).

[40] F. Almyahi, T.R. Andersen, A. Fahy, M. Dickinson, K. Feron, W.J. Belcher, P.C. Dastoor, The role of surface energy control in organic photovoltaics based on solar paints, Journal of Materials Chemistry A. 7 (2019) 9202–9214. https://doi.org/10.1039/c8ta09521c.

[41] H. Guo, T. Shen, F. Wu, G. Wang, L. Ye, Z. Liu, B. Zhao, S. Tan, Controlling the morphology and hole mobility of terpolymers for polymer solar cells, RSC Advances. 6 (2016) 13177–13184. https://doi.org/10.1039/c5ra23863c.

[42] Burgués-Ceballos, F. Hermerschmidt, A. V. Akkuratov, D.K. Susarova, P.A. Troshin, S.A. Choulis, High-Performing Polycarbazole Derivatives for Efficient Solution-Processing of Organic Solar Cells in Air, ChemSusChem. 8 (2015) 4209–4215. https://doi.org/10.1002/cssc.201501128.

Acknowledgments

The authors are indebted to the CAPES and CEPEL for financial support.

Supplementary Interactive Plot Data (CSV)

Declaration of interests

☒ The authors declare that they have no known competing financial interests or personal relationships that could have appeared to influence the work reported in this paper.

☐The authors declare the following financial interests/personal relationships which may be considered as potential competing interests:

Declarations of interest: none